

Electronic Supplementary Information for

Designing the Crystalline Structure of Calcium Phosphate Seed Minerals in Organic Templates for Sustainable Phosphorus Management

Doyoon Kim,^a Tong Wu,^a Melanie Cohen,^a Inhyeong Jeon^{a,b} and Young-Shin Jun^{*a}

^a Department of Energy, Environmental & Chemical Engineering,
Washington University in St. Louis, St. Louis, Missouri 63130, United States

^b Department of Civil & Environmental Engineering, Seoul National University,
Seoul 08826, Republic of Korea

**E-mail: ysjun@seas.wustl.edu*

The electronic supplementary information consists of total 17 pages, including 1 table and 7 figures.
See the detailed contents below.

Contents:

S1. A case study: Hydroxyapatite saturation index mapping of groundwater	S2
S2. Characterizations of beads	S7
S3. Thermodynamic calculations of Ca and P concentrations in equilibrium with different calcium phosphate minerals	S10
S4. Potential formation of struvite in the HA-supersaturated condition	S14
S5. Aqueous Fe and P concentrations equilibrated with hematite and strengite	S15
S6. P removal using Ca-Alg/CaP over 3 cycles of batch experiments	S16
References	S17

S1. A case study: Hydroxyapatite saturation index (SI) mapping of groundwater in the Chesapeake Bay, Louisiana, and northern Illinois areas

A. Procedures. This study was conducted to test our hypothesis that many nutrient-rich environments are already supersaturated with respect to hydroxyapatite (HA). If we are able to cause such aqueous systems to reach equilibrium quickly (e.g., by adding calcium phosphate (CaP) seed nuclei in calcium alginate beads, as used in this study), we can easily regulate the P concentration at a lower level, reducing the risk of eutrophication. In this case study, we investigated the actual SI values (the log of the ion activity product, *IAP*, divided by the solubility product, K_{sp}) of groundwater samples from three areas in the USA. The Chesapeake Bay area (C. Bay) was chosen because of the frequent occurrence of eutrophication in this region due to inflows from natural and anthropogenic sources.^{1,2} Similarly, the coastal Louisiana area (LA) has also faced issues associated with eutrophication and high P levels in the water.³ Contrarily, an area in northern Illinois area (IL) near Lake Michigan was chosen because of this region's reputation for low P levels,⁴ but this area may show relatively high Ca levels due to its calcareous soils.⁵

Groundwater monitoring data (1970–2007) were collected from the USGS National Groundwater Monitoring Network (NGWMN),⁶ then processed to determine whether environments were actually supersaturated with respect to HA (HA-supersaturated). The latest data from groundwater samples, including pH, total P (assumed to be equal to total phosphate) concentration, hardness, and total dissolved solid values, were selected as input parameters for Visual MINTEQ (Ver. 3.1), which calculates the SI using its built-in database. Hardness data (as CaCO_3) were used as input parameters of Ca^{2+} , unless Ca^{2+} concentration was given specifically. The concentrations of Ca^{2+} , aqueous carbonate species, Na^+ , and Cl^- were considered to calculate the ionic strength. By assuming that the amount of total dissolved solids is the sum of the hardness

and NaCl, we estimated the concentrations of NaCl. Organic molecules, such as natural organic matter and extracellular matrix proteins from microorganisms, may influence the saturation condition or nucleation energy barrier by complexation with Ca^{2+} or other aqueous species.^{7,8} However, in this proof of concept calculation, we limited the input parameters to the inorganic compounds listed above. The SI values for HA, as the output parameters of the software, were placed on SI maps (Fig. S1a-c) created by ArcGIS (Esri, USA), using longitude and latitude information from the NGWMN database.⁶

B. Analyses of SI of three areas. Based on our thermodynamic calculations of the SI values for HA, interestingly, 36 out of 48 groundwater samples (75%) in the C. Bay area were HA-supersaturated (Fig. S1a). Most of the HA-supersaturated sampling points were close to the Bay, indicating that significant Ca and P concentrations have been introduced into the ocean through the groundwater. Two sampling sites were studied from LA, and the SI values of both sites were higher than 4 (Fig. S1b). Because of the limited data available, the result may not represent the entire LA area. However, this result also shows that multiple aqueous environments are HA-supersaturated. In contrast, only two out of five sites were slightly HA-supersaturated ($0 < \text{SI} < 2$) in northern IL, and other three sites were undersaturated with respect to HA ($\text{SI} < 0$, Fig. S1c).

The SI values in the three studied areas show correlations in the order $\text{pH} > \text{P} > \text{Ca}$ (Fig. S2a–c). P concentrations in C. Bay and LA are obviously higher than in northern IL (Fig. S2d), suggesting the influence of increasing P levels on eutrophication. Due to the calcareous soils, Ca concentrations in the northern IL are relatively higher than in the other two areas (Fig. S2e). However, due to the region's low P concentrations and pH, SI values are relatively low (Fig. S1c). The pH values for the HA-supersaturated sites are typically higher than 7 (Fig. S2f), and HA is the

most stable of calcium phosphate minerals in this pH range.⁹ Our study shows that Ca-Alg/CaP can effectively decrease P concentrations close to the equilibrium level with HA at pH around 7 (Fig. 6). Therefore, this strategy can contribute to maintaining the P level in the stable range (e.g., equilibrium with seed mineral in beads), preventing a sudden increase of P in the aqueous systems.

Based on the evaluation of SI for HA in areas with high eutrophication risks (C. Bay and LA) and the comparison with an area relatively free from the risk (IL), we suggested that utilizing the thermodynamic property of HA (i.e., its low solubility at neutral pH) can advantageously regulate P concentrations in most aqueous systems. In addition, to select other possible application sites, we can refer to the USGS database.

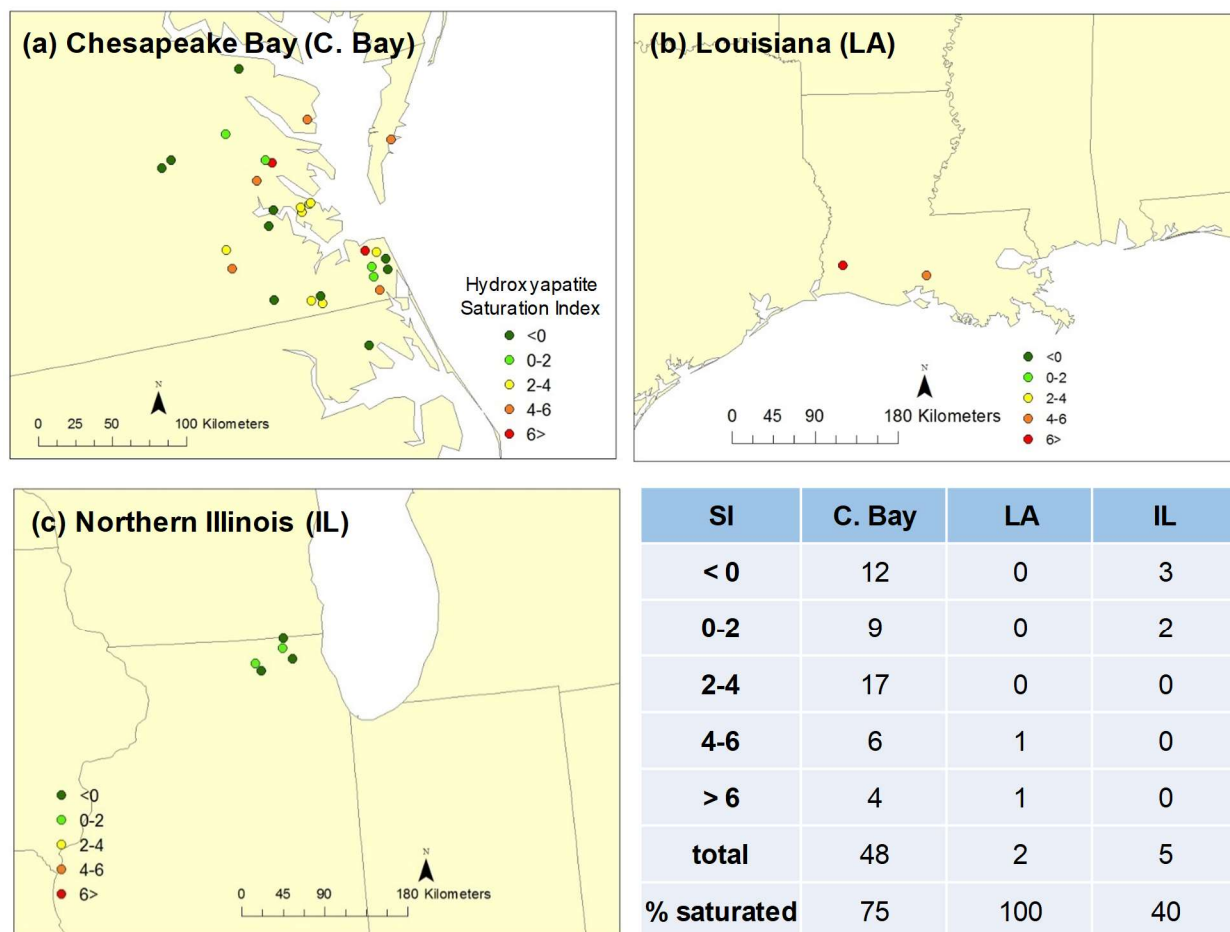


Fig. S1. Hydroxyapatite SI maps of the (a) Chesapeake Bay (C. Bay), (b) Louisiana (LA), and (c) northern Illinois (IL) areas. The SI values were calculated using Visual MINTEQ. The table at the bottom right corner summarizes the number of sampling sites categorized into different SI values.

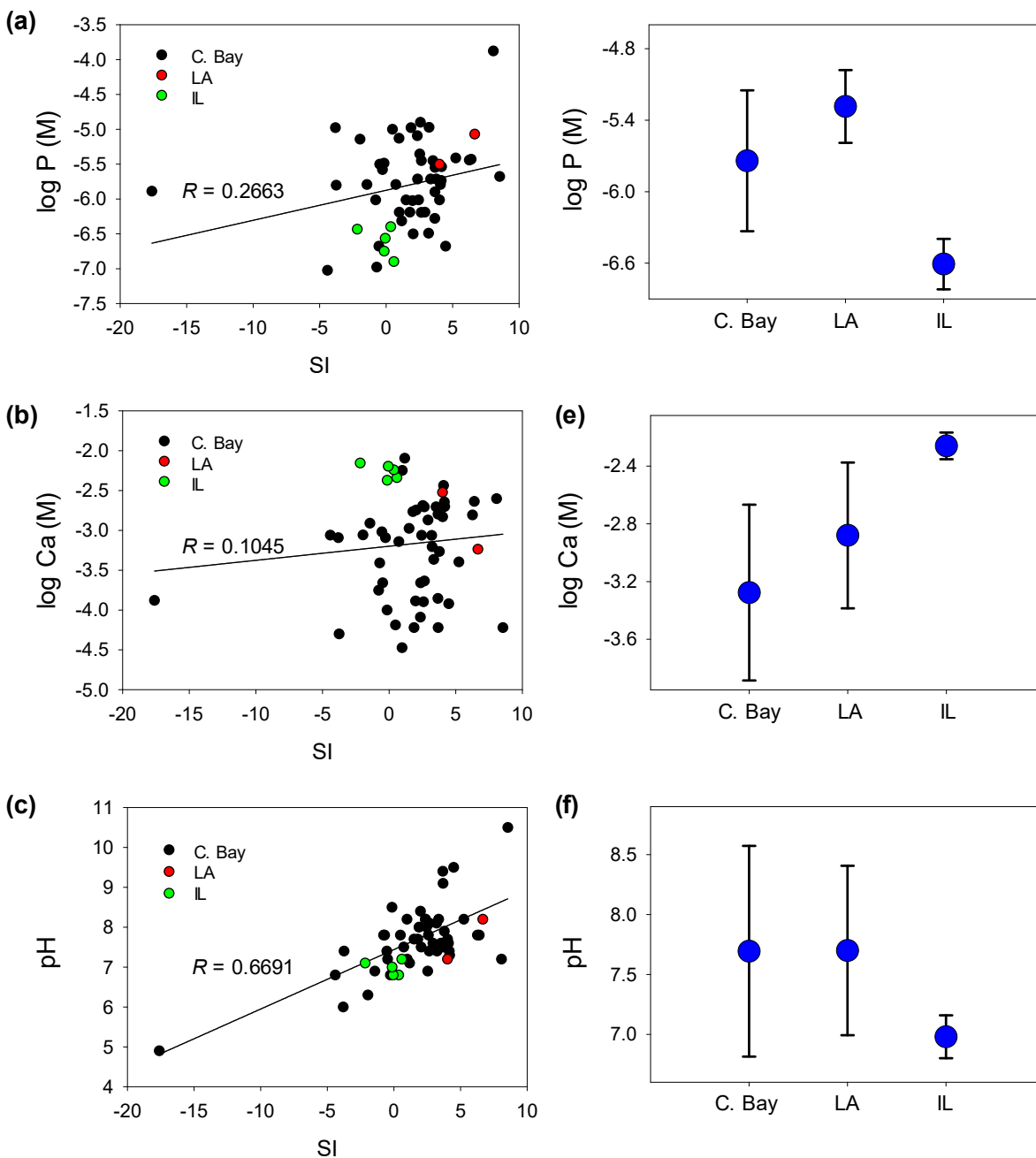


Fig. S2. (a-c) Relationships between the SI for HA and concentrations of P, Ca, and pH in three areas studied (C. Bay, Chesapeake Bay; LA, Louisiana; IL, northern Illinois). R is the correlation coefficient from the linear relationship. (d-f) Average and standard deviation values of P, Ca, and pH in these three areas are shown separately in the right column figures.

S2. Characterizations of beads

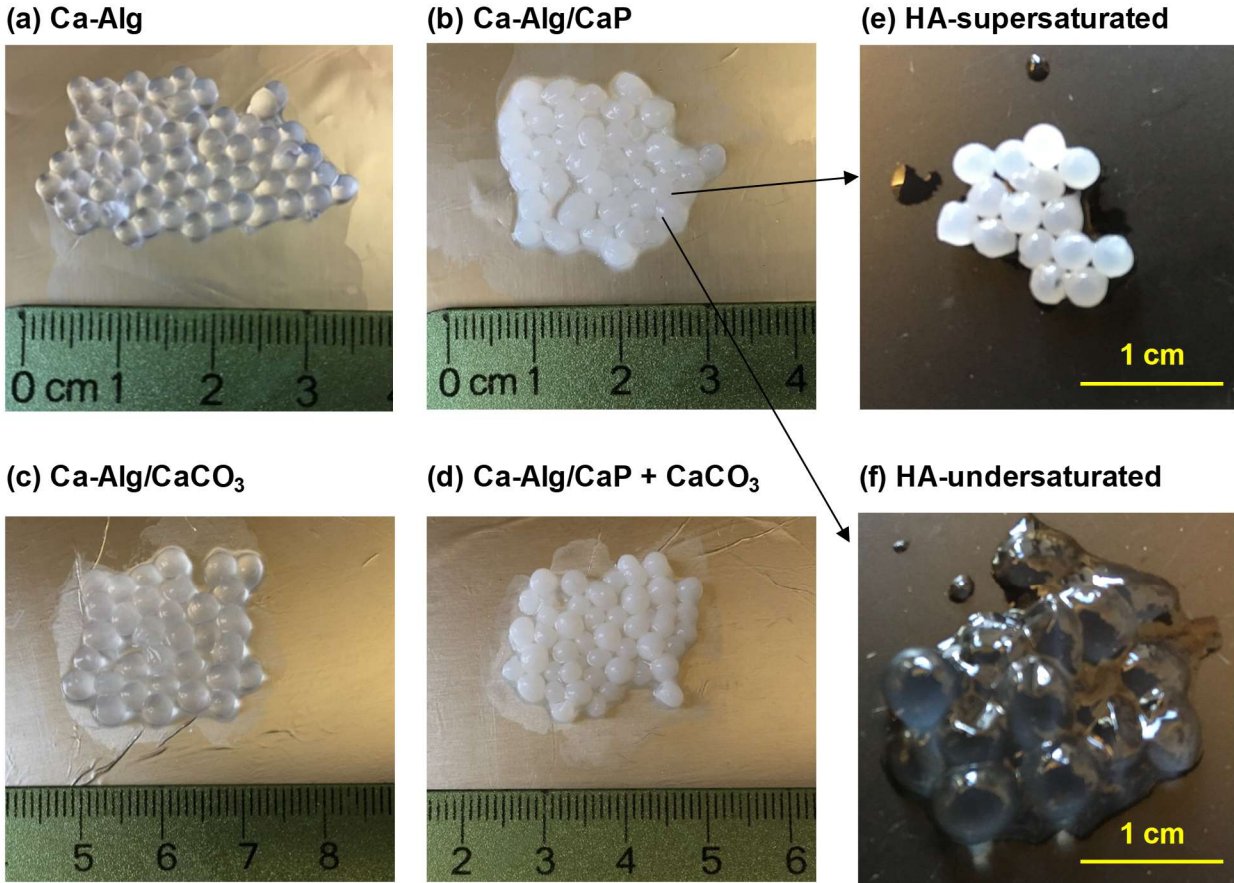


Fig. S3. (a-d) Photographs of the four different types of beads used in this study. (e-f) Ca-Alg/CaP after three cycles of P removal experiments (24 hours for one cycle) under HA-supersaturated and HA-undersaturated conditions.

Table S1. Bead sizes and dry weights of beads and seed minerals.

	Ca-Alg	Ca-Alg/CaP	Ca-Alg/CaCO ₃	Ca-Alg/CaP+CaCO ₃
Bead size (mm)	2.8 ± 0.2	3.3 ± 0.4	3.8 ± 0.2	3.2 ± 0.4
Dry weight (mg)*	14.0 ± 3.9	19.7 ± 1.7	19.4 ± 1.3	24.7 ± 2.0
Seed weight (mg)	-	5.7	5.5	10.7

*Drying procedure is described below.

To analyze the particle sizes, ImageJ 1.47v (National Institutes of Health, USA) was used. The average and standard deviation values for each bead type were obtained by measuring 15 samples. For the batch experiments for P removal, 2 mL of sodium alginate solution (6 mg L^{-1}) was added dropwise to form beads. The average and standard deviation of the dry weight were obtained from triplicate bead preparation procedures. Beads were fully dried in a 105°C oven for 24 hours before the measurements. The dry weights of Ca-Alg beads were slightly higher than the amount of initially added sodium alginate (12 mg) because of calcium replacement and structural water inside the composites. The dry weights of seed minerals were calculated by subtracting that of Ca-Alg beads.

A. Procedures for other characterizations of beads and seed minerals. Before and after the P removal experiments, to characterize the crystalline structure of seed minerals and to image the surfaces of beads, X-ray diffraction (XRD, Bruker D8 Advance) data and scanning electron microscope (SEM, FEI Nova NanoSEM 2300) images of beads were used, respectively. To prepare samples for XRD and SEM analyses, beads were air-dried and gently ground with ethanol in an agate mortar. For XRD analysis, ground samples were placed on a zero diffraction Si plate (MTI Corporation), then the XRD patterns were collected using $\text{Cu K}\alpha$ radiation (40 kV and 40 mA). For SEM analysis, ground samples were placed on adhesive carbon tapes attached on SEM stubs, sputter-coated with Au-Pd under Ar gas at 0.2 mbar (Cressington 108) to increase conductivity, then imaged with a 10 kV electron accelerating voltage at 5–6 mm working distances.

To characterize the particle size and crystallinity of CaP seed nuclei prepared with different OH^- concentrations, X-ray scattering data were collected at the Advanced Photon Source (APS) at Argonne National Laboratory (Argonne, IL, USA). Beads were packed in Kapton polyimide capillaries (Cole-Parmer, inner diameter 1.46 mm) without any dehydration procedures. Analyses

of samples under hydrated conditions maintained the particle sizes and phases of CaP nuclei. Wide-angle X-ray diffraction (WAXD) and X-ray pair distribution function (PDF) data were collected at sector 11-ID-B using a 58.66 keV X-ray beam.¹⁰ For the WAXD data collection, samples were exposed to the beam for 25 sec at a sample-to-detector distance (SDD) of 95 cm. For the X-ray PDF, data was collected during 3 min of beam exposure using a 20 cm SDD. Then one-dimensional data were produced by using FIT2D software provided by European Synchrotron Radiation. The PDF function, $G(r)$, was obtained by PDFgetX2 software to provide the atomic number density as a function of atomic separation distances, r .¹¹ We evaluated particle size (d) over a wide range of the scattering vector, $q = 0.0001\text{--}0.1 \text{ \AA}^{-1}$, using ultra-small-angle X-ray scattering (USAXS). Because $d = 2\pi/q$, the corresponding particle size range was 6.3 nm–6.3 μm . USAXS data was collected at sector 9-ID-C using a 21.0 keV X-ray beam.¹² Data analyses, including one-dimensional data reduction and fitting scattering patterns, were conducted using a series of macro programs in the IRENA package written in IGOR Pro (WaveMetrics Inc.), which was provided by sector 9-ID-C.¹³⁻¹⁵ In addition, SAXS measurements of samples were conducted at sector 12-ID-B (14.0 keV) to better evaluate the features of small particles appearing at $q = 0.009\text{--}0.3 \text{ \AA}^{-1}$ ($d = 2\text{--}70 \text{ nm}$). The WAXD, USAXS, and SAXS patterns of an empty Kapton capillary were also collected for background subtraction.

S3. Thermodynamic calculations of Ca and P concentrations in equilibrium with different calcium phosphate minerals

The concentrations of Ca and P species equilibrated with different calcium phosphate minerals at pH 5–10 were calculated based on the equilibrium constants among calcium, phosphate, and carbonate species. To simulate the calcium phosphate saturated condition used in this study, 10 mM NaCl, 2 mM CaCl₂, and 0.2 mM Na₂HPO₄ were added as initial aqueous components, and an open carbonate system ($p_{CO_2} = 10^{-3.5}$, $p_{CO_2}/[H_2CO_3(aq)] = 31.6$ atm/M) was assumed. The association/dissociation reactions listed in eq. 1–11 were considered for the calculation of the activities of carbonate, phosphate, and calcium species in the system.^{16,17}

$$K_{A1,CO_3} = \frac{(H^+)(HCO_3^-)}{(H_2CO_3(aq))} = 10^{-6.35} \quad \text{eq. 1}$$

$$K_{A2,CO_3} = \frac{(H^+)(CO_3^{2-})}{(HCO_3^-)} = 10^{-10.33} \quad \text{eq. 2}$$

$$K_{A1,PO_4} = \frac{(H^+)(H_2PO_4^-)}{(H_3PO_4(aq))} = 10^{-2.12} \quad \text{eq. 3}$$

$$K_{A2,PO_4} = \frac{(H^+)(HPO_4^{2-})}{(H_2PO_4^-)} = 10^{-7.21} \quad \text{eq. 4}$$

$$K_{A3,PO_4} = \frac{(H^+)(PO_4^{3-})}{(HPO_4^{2-})} = 10^{-12.32} \quad \text{eq. 5}$$

$$K_{CaHCO_3^+} = \frac{(CaHCO_3^+)}{(Ca^{2+})(HCO_3^-)} = 10^{1.16} \quad \text{eq. 6}$$

$$K_{CaCO_3(aq)} = \frac{(CaCO_3(aq))}{(Ca^{2+})(CO_3^{2-})} = 10^{3.38} \quad \text{eq. 7}$$

$$K_{CaOH^+} = \frac{(CaOH^+)}{(Ca^{2+})(OH^-)} = 25.12 \quad \text{eq. 8}$$

$$K_{CaH_2PO_4^+} = \frac{(CaH_2PO_4^+)}{(Ca^{2+})(H_2PO_4^-)} = 31.9 \quad \text{eq. 9}$$

$$K_{CaHPO_4(aq)} = \frac{(CaHPO_4(aq))}{(Ca^{2+})(HPO_4^{2-})} = 6.81 \times 10^2 \quad \text{eq. 10}$$

$$K_{\text{CaPO}_4^-} = \frac{(\text{Ca}^{2+})(\text{PO}_4^{3-})}{(\text{CaPO}_4^-)} = 3.46 \times 10^6 \quad \text{eq. 11}$$

The activity of each ionic component, i , in parentheses was the product of its concentration, C_i , and the activity coefficient of the component, γ_i by the Davies equation (eq. 12). I is the ionic strength of the solution (eq. 13) and Z is the charge of the component.¹⁷

$$\log \gamma_i = -0.5 Z_i^2 \left[\frac{\frac{1}{I^2}}{1 + \frac{1}{I^2}} - 0.2I \right] \quad \text{eq. 12}$$

$$I = \frac{1}{2} \sum_i c_i Z_i^2 \quad \text{eq. 13}$$

By applying eqs. 1–13 to mass balance equations with respect to Ca, PO_4^{3-} , and CO_3^{2-} , we calculated the activities of all components and the IAP of three different calcium phosphate minerals: HA (eq. 14), octacalcium phosphate (OCP, eq. 15), and dicalcium phosphate (DCP, eq. 16). In addition to these calcium phosphate minerals, the most stable calcium carbonate mineral, calcite (CC, eq. 17), was considered as well, due to the higher possibility of its formation in an aqueous system with a sufficient amount of Ca in a high pH range.

$$IAP_{\text{HA}} = (\text{Ca}^{2+})^5 (\text{PO}_4^{3-})^3 (\text{OH}^-) \quad \text{eq. 14}$$

$$IAP_{\text{OCP}} = (\text{Ca}^{2+})^4 (\text{H}^+) (\text{PO}_4^{3-})^3 \quad \text{eq. 15}$$

$$IAP_{\text{DCP}} = (\text{Ca}^{2+}) (\text{HPO}_4^{2-}) \quad \text{eq. 16}$$

$$IAP_{\text{CC}} = (\text{Ca}^{2+}) (\text{CO}_3^{2-}) \quad \text{eq. 17}$$

The SI for each mineral can be calculated by IAP over K_{sp} in log scale ($\text{SI} = \log \frac{IAP}{K_{sp}}$). The experimentally determined K_{sp} values were obtained from different literature sources: $K_{sp, \text{HA}} =$

$10^{-58.5}$ at 25°C ,¹⁸ $K_{\text{sp,OCP}} = 10^{-48.4}$ at 23.5°C ,¹⁹ $K_{\text{sp,DCP}} = 10^{-6.62}$ at 25°C ,²⁰ and $K_{\text{sp,CC}} = 10^{-8.48}$ at 25°C .²¹ SI values were evaluated for each mineral at each pH, from 5 to 10 with 0.05 steps. When $\text{SI} > 0$, we assumed that phosphate (or carbonate for CC) species were governed by K_{sp} reaching an equilibrium. Thus concentrations of all the species were recalculated until the sum of Ca precipitated as a mineral and all the aqueous Ca species equaled the initial Ca amount in the system. The computational work was done using a script written in MATLAB R2013 (Mathworks, USA).

Fig. S4a,b show the total aqueous Ca and P concentrations, equilibrated with different calcium phosphate and carbonate minerals at pH 5–10. Fig. S4c shows the SI with respect to different calcium phosphate minerals. Among the minerals studied, HA shows the lowest solubility above pH 6. Aqueous P concentration starts to decrease at pH 7, when equilibrium with OCP is reached. However, the system is undersaturated with respect to dicalcium phosphate within the pH range evaluated. Calcite formation becomes significant above pH 8, and therefore, carbonate may compete with phosphate for Ca above that pH. However, the equilibrium pH values of the solution after the experiments in this study were all below pH 8, thus the possibility of CC formation was considered insignificant.

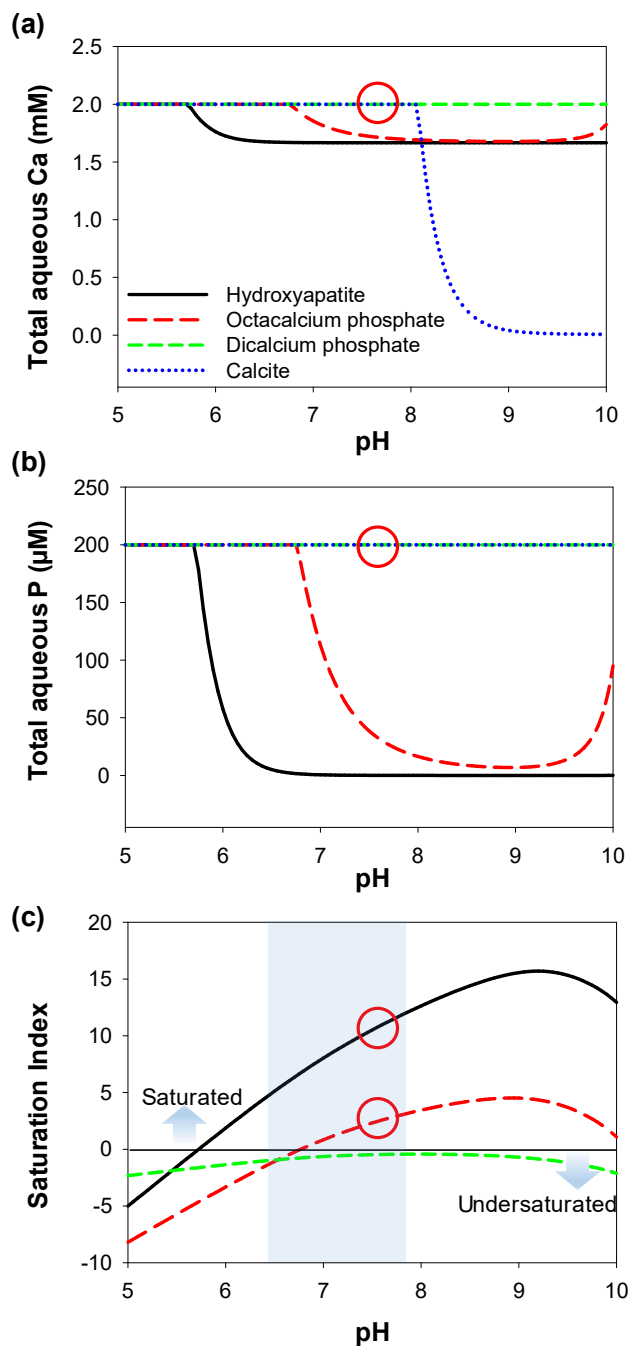


Fig. S4. Ca and P concentrations in equilibrium with different calcium phosphate and carbonate minerals at pH 5–10 (a-b). Initial conditions of the system: 10 mM NaCl, 2 mM CaCl₂, and 0.2 mM Na₂HPO₄. Open carbonate system. Plotted saturation indices for calcium phosphate minerals under the initial condition in the pH range (c). The blue box in (c) highlights the experimental regime used in this study. Red circles in (a-c) indicate the initial experimental condition for P removal experiments in the saturated system.

S4. Potential formation of struvite in the HA-supersaturated condition

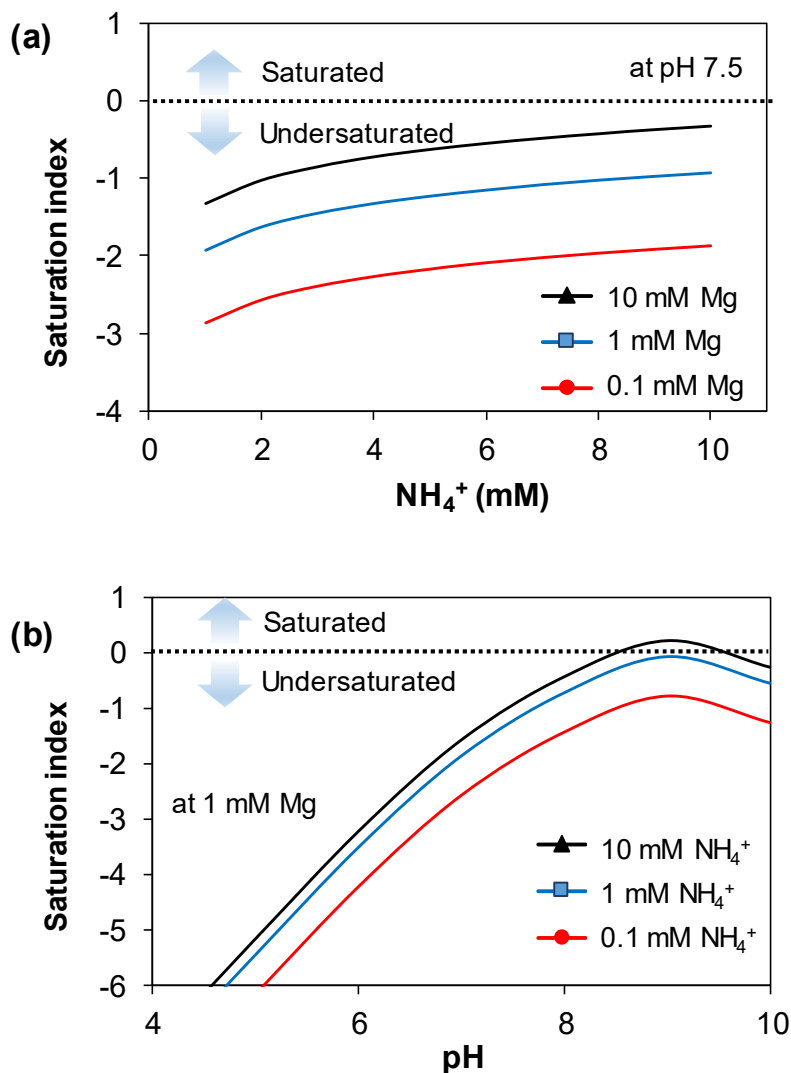


Fig. S5. Supersaturation index with respect to struvite in the HA-supersaturated condition. (a) The influence of NH_4^+ at 0.1–10 mM Mg in the system. (b) The influence of pH at 0.1–10 mM NH_4^+ . Thermodynamic equilibrium calculations were conducted by Visual MINTEQ (Ver. 3.1). Our simulation result shows that in most cases, even at high Mg^{2+} and NH_4^+ concentrations up to 10 mM, the HA-supersaturated solution was undersaturated with respect to struvite at neutral pH. For comparison, typical levels of NH_4^+ in toilet water²² and Mg^{2+} in fresh urine²³ are around 5 and 4 mM, respectively.

S5. Aqueous Fe and P concentrations equilibrated with hematite and strengite

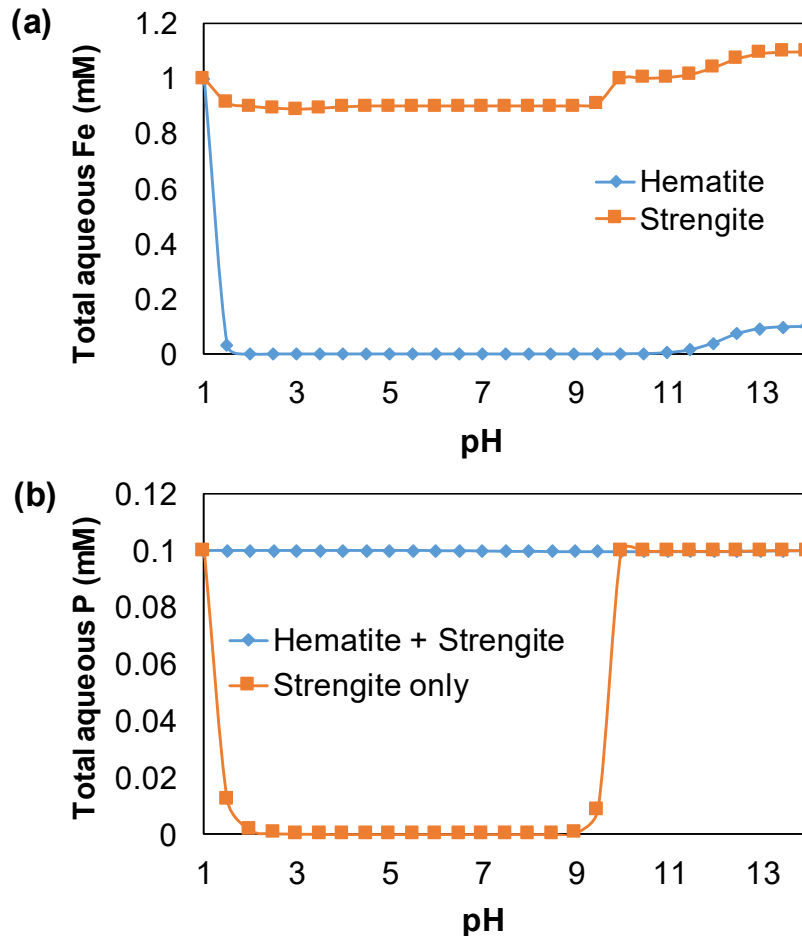


Fig. S6. Aqueous Fe and P concentrations equilibrated with hematite (Fe_2O_3) and strengite ($\text{FePO}_4 \cdot 2\text{H}_2\text{O}$). Thermodynamic equilibrium calculations were conducted by Visual MINTEQ (Ver. 3.1). Initial conditions of the system were 1 mM FeCl_3 and 0.1 mM Na_3PO_4 . A lower Fe concentration equilibrated with hematite than with strengite indicates that iron oxide is more thermodynamically stable than iron phosphate minerals (a). If hematite precipitation occurs (b), the immobilization of P as a strengite mineral is inhibited. At higher pH, iron hydroxide formation dominates, therefore P immobilization is also inhibited.

S6. P removal using Ca-Alg/CaP over 3 cycles of batch experiments

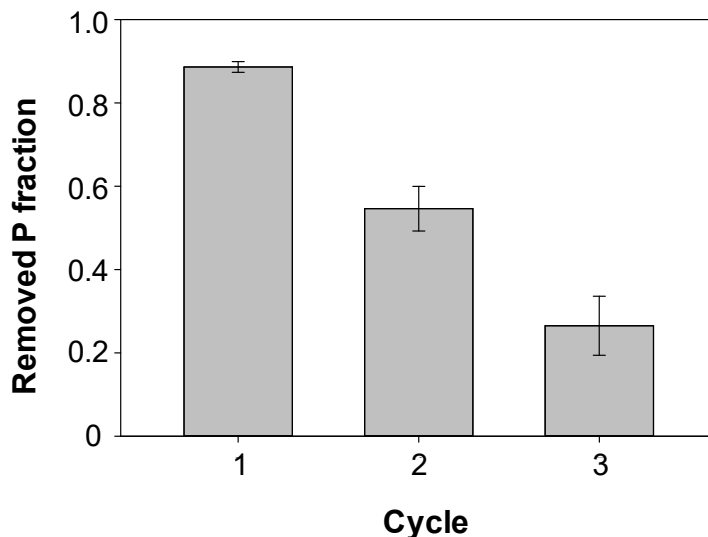


Fig. S7. Removed P fractions in solutions (initial conditions were 10 mM NaCl, 0.2 mM Na₂HPO₄, and 2 mM CaCl₂, pH = 7.8) using Ca-Alg/CaP. Experiments were conducted by adding beads prepared by addition of 2 mL sodium alginate solution (equivalent to 5.7 mg of dry CaP seed mineral, see Section S2) into a batch containing 100 mL solution (first cycle). After 24 hours of reactions, beads were collected and then transferred to a fresh batch (second cycle). Three batches were used for removal with the same beads.

References

1. J. D. Hagy, W. R. Boynton, C. W. Keefe and K. V. Wood, *Estuaries*, 2004, **27**, 634-658.
2. N. N. Rabalais, R. E. Turner, R. J. Díaz and D. Justić, *ICES J. Mar. Sci.*, 2009, **66**, 1528-1537.
3. N. N. Rabalais, R. E. Turner, B. K. S. Gupta, E. Platon and M. L. Parsons, *Ecol. Appl.*, 2007, **17**, S129-S143.
4. C. L. Schelske, E. F. Stoermer and W. F. Kenney, *Limnol. Oceanogr.*, 2006, **51**, 728-748.
5. E. K. Read, M. Ivancic, P. Hanson, B. J. Cade-Menun and K. D. McMahon, *Water Res.*, 2014, **62**, 229-240.
6. National Ground-Water Monitoring Network Website, <http://cida.usgs.gov/ngwmn/index.jsp>.
7. M. J. Olszta, X. Cheng, S. S. Jee, R. Kumar, Y.-Y. Kim, M. J. Kaufman, E. P. Douglas and L. B. Gower, *Mater. Sci. Eng. R*, 2007, **58**, 77-116.
8. X. Cao, W. G. Harris, M. S. Josan and V. D. Nair, *Sci. Total Environ.*, 2007, **383**, 205-215.
9. O. Borkiewicz, J. Rakovan and C. L. Cahill, *Am. Mineral.*, 2010, **95**, 1224-1236.
10. K. W. Chapman, S. H. Lapidus and P. J. Chupas, *J. Appl. Crystallogr.*, 2015, **48**.
11. X. Qiu, J. W. Thompson and S. J. Billinge, *J. Appl. Crystallogr.*, 2004, **37**, 678-678.
12. J. Ilavsky, F. Zhang, A. J. Allen, L. E. Levine, P. R. Jemian and G. G. Long, *Metal. Mater. Trans A*, 2013, **44**, 68-76.
13. J. Ilavsky, P. R. Jemian, A. J. Allen, F. Zhang, L. E. Levine and G. G. Long, *J. Appl. Crystallogr.*, 2009, **42**, 469-479.
14. J. Ilavsky and P. R. Jemian, *J. Appl. Crystallogr.*, 2009, **42**, 347-353.
15. F. Zhang, J. Ilavsky, G. Long, J. G. Quintana, A. Allen and P. Jemian, *Metall. Mater. Trans. A*, 2010, **41**, 1151-1158.
16. X. Lu and Y. Leng, *Biomaterials*, 2005, **26**, 1097-1108.
17. C. N. Sawyer, P. L. McCarthy and G. F. Parkin, *Chemistry for Environmental Engineering and Science*, McGraw Hill, 2002.
18. H. McDowell, T. Gregory and W. Brown, *J. Res. Nat. Bur. Stand. A*, 1977, **81**, 273-281.
19. M. Tung, N. Eidelman, B. Sieck and W. Brown, *J. Res. Nat. Bur. Stand.*, 1988, **93**, 613-624.
20. T. M. Gregory, E. C. Moreno and W. E. Brown, *J. Res. Nat. Bur. Stand. A*, 1970, **74A**, 461-475.
21. L. N. Plummer and E. Busenberg, *Geochim. Cosmochim. Acta*, 1982, **46**, 1011-1040.
22. X. Huang, Y. Qu, C. A. Cid, C. Finke, M. R. Hoffmann, K. Lim and S. C. Jiang, *Wat. Res.*, 2016, **92**, 164-172.
23. K. A. Landry, P. Sun, C.-H. Huang and T. H. Boyer, *Wat. Res.*, 2015, **68**, 510-521.